# High spin states in $^{206,204,202}$Tl observed in $(d,\alpha)$ reactions at 80 MeV*

N. Frascaria
*Institut de Physique Nucléaire, BP 1, 91406 Orsay, France*

J. P. Didelez†
*University of Maryland, College Park, Maryland*
*and Institut für Kernphysik der Kernforschungsanlage, Jülich D-5170 Germany*

N. S. Chant and C. C. Chang
*University of Maryland, College Park, Maryland 20742*

(Received 3 December 1976)

The $(d,\alpha)$ reaction on $^{208,206,204}$Pb has been studied at 80 MeV bombarding energy. The experimental angular distributions are structured and the transferred angular momentum $L$ could be determined without ambiguity from a comparison of distorted-wave Born-approximation calculations with the experimental angular distributions. The angular momentum matching conditions greatly favored large values of $L$ and allowed the identification of $J^\pi = 12^-$ and $9^+$ states in $^{206,204,202}$Tl. Data for the $^{208}$Pb$(d,\alpha)^{206}$Tl reaction were compared with shell model calculations. The properties of nine levels could be correlated with very good agreement with those of states predicted in the shell model calculations. Both zero-range and exact finite-range distorted-wave Born-approximation calculations were carried out. Unlike the zero-range distorted-wave Born-approximation results, the exact finite-range angular distributions did not change greatly for different choices of the $\alpha$ particle optical potential. Although somewhat better agreement with the relative cross sections was obtained, the exact finite-range calculations underestimated the absolute cross sections by roughly a factor of 50.

[NUCLEAR REACTIONS $^{208,206,204}$Pb$(d,\alpha)$, $E_d = 80$ MeV. Measured $\sigma(\theta)$; enriched targets; microscopic DWBA analysis; shell model calculations; deduced $J,\pi$.]

## I. INTRODUCTION

Direct $(d,\alpha)$ reactions performed on $0^+$ targets have proved to be highly selective.[1] At high incident energy the requirement of good angular momentum matching strongly favors high angular momenta $L$ for the transferred nucleon pair. As a result of this kinematical constraint it is anticipated that a few high spin states will be preferentially excited in the residual nuclei. Thus, one might hope to utilize this special selectivity to resolve high spin states in regions of high level density.

From the shell model point of view two particle pickup reactions are also of particular interest for the study of odd-odd nuclei in the lead region since the doubly magic $^{208}$Pb nucleus can be regarded as a closed core[2] and the $(d,\alpha)$ reaction allows the study of fairly simple proton-neutron hole states in the residual nucleus. Specifically, experimental results can be used to test the theoretical predictions of the large basis shell model calculations carried out by Kuo and Herling.

For the above mentioned reasons we have investigated the $(d,\alpha)$ reaction on $^{208}$Pb, $^{206}$Pb, and $^{204}$Pb at 80 MeV incident energy. In addition, by comparing experimental data for these three isotopes we have attempted to provide information on spin assignments in $^{206,204,202}$Tl and also study the effect of the addition of neutron holes.

In previous studies, the low-lying levels of $^{206}$Tl have been investigated with the $(d,\alpha)$ reaction[4] at low energy and some additional information is available from the study of $(d,p)$ and $(t,\alpha)$ reactions.[5,6] In addition, some few low-lying excited states have been seen in radiative $\alpha$-decay[7] and neutron capture studies.[8] Presently, very few studies of $^{202}$Tl and $^{204}$Tl have been done.[9,10]

In this paper we first present the experimental method and results. We next describe microscopic distorted-wave Born-approximation (DWBA) calculations using both zero range (ZR) and exact finite range (EFR) approaches. Finally we compare our data with DWBA calculations using shell model wave functions[3] and discuss spin assignments.

## II. EXPERIMENTAL METHOD

The $(d,\alpha)$ reactions were induced by the 80 MeV analyzed deuteron beam from the University of Maryland isochronous cyclotron. For a maximum beam intensity of 100 nA in the scattering chamber (as measured by a Faraday cup) the beam en-

ergy spread was of the order of 30 keV.

Outgoing $\alpha$ particles were detected by a conventional detector telescope consisting of 500 $\mu$m Si surface barrier $\Delta E$ detector followed by a 3000 $\mu$m Si(Li)$E$ detector. In addition, a 1000 $\mu$m silicon surface barrier detector located behind the $E$ detector provided a veto signal in order to reduce, by means of a fast coincidence-anticoincidence unit, the high counting rate due to the intense flux of elastically scattered deuterons. Finally, a pileup gate, feeding a second fast coincidence-anticoincidence unit, rejected any pair of signals occurring in the $E$ detector within 300 ns and allowed a reasonably high counting rate without appreciable deterioration of the resolution.

Data were analyzed on line by an IBM 360/44 computer with the particle identification program GELIAN of the University of Maryland Cyclotron Laboratory and the identified energy spectra corresponding to $^3$He and $\alpha$ particles were written on tape after each measurement.

## III. EXPERIMENTAL RESULTS

With the above described experimental setup and targets with thicknesses in the range of 1 mg/cm$^2$ an overall energy resolution of 100 keV could be achieved. Typical $\alpha$ spectra are shown in Fig. 1 for the $^{208,206,204}$Pd($d$, $\alpha$)$^{206,204,202}$Tl reactions at 10° laboratory angle.

Differential cross sections were measured between 6° and 30° laboratory angle in 3° steps. Angular distributions grouped according to similarity in shape are shown in Figs. 2–4. The assigned error bars include statistical and background subtraction uncertainties. The absolute error due to target thickness, solid angle, and beam monitoring uncertainties is approximately 10%.

The three spectra of Fig. 1 have several common features:

(i) In each spectrum a few states located around 2.5 MeV excitation energy are strongly populated and have similar angular distributions for the three Tl isotopes.

(ii) The states significantly excited appear at a rather low excitation energy (below ~3.5 MeV). Since the incident energy is large compared to the Coulomb barrier one might expect to observe levels at excitation energy as high as 8 MeV as in our previous work on $1f_{7/2}$ shell nuclei.[1] A similar hindrance effect affecting the higher excitation energy region was already pointed out by Lewis and Daehnick[4] in their very complete study of the $^{208}$Pb($d$, $\alpha$)$^{206}$Tl reaction at low energy (17 MeV). These authors suggested that not only the Coulomb barrier but also destructive interference between the various hole configurations involved could explain this feature.

(iii) The measured differential cross sections are surprisingly large (of the order of 100 $\mu$b/sr at 10° for the above mentioned most strongly excited states).

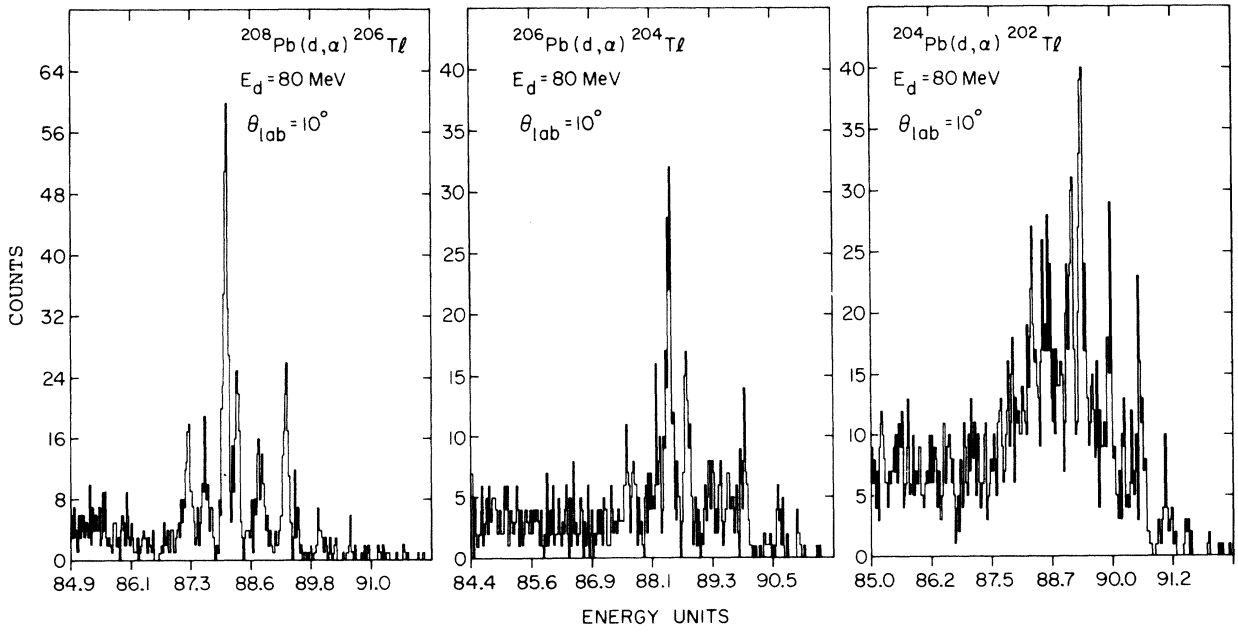


FIG. 1. Energy spectra of $\alpha$ particles from $^{208,206,204}$Pb+$d$ reactions at 80 MeV.

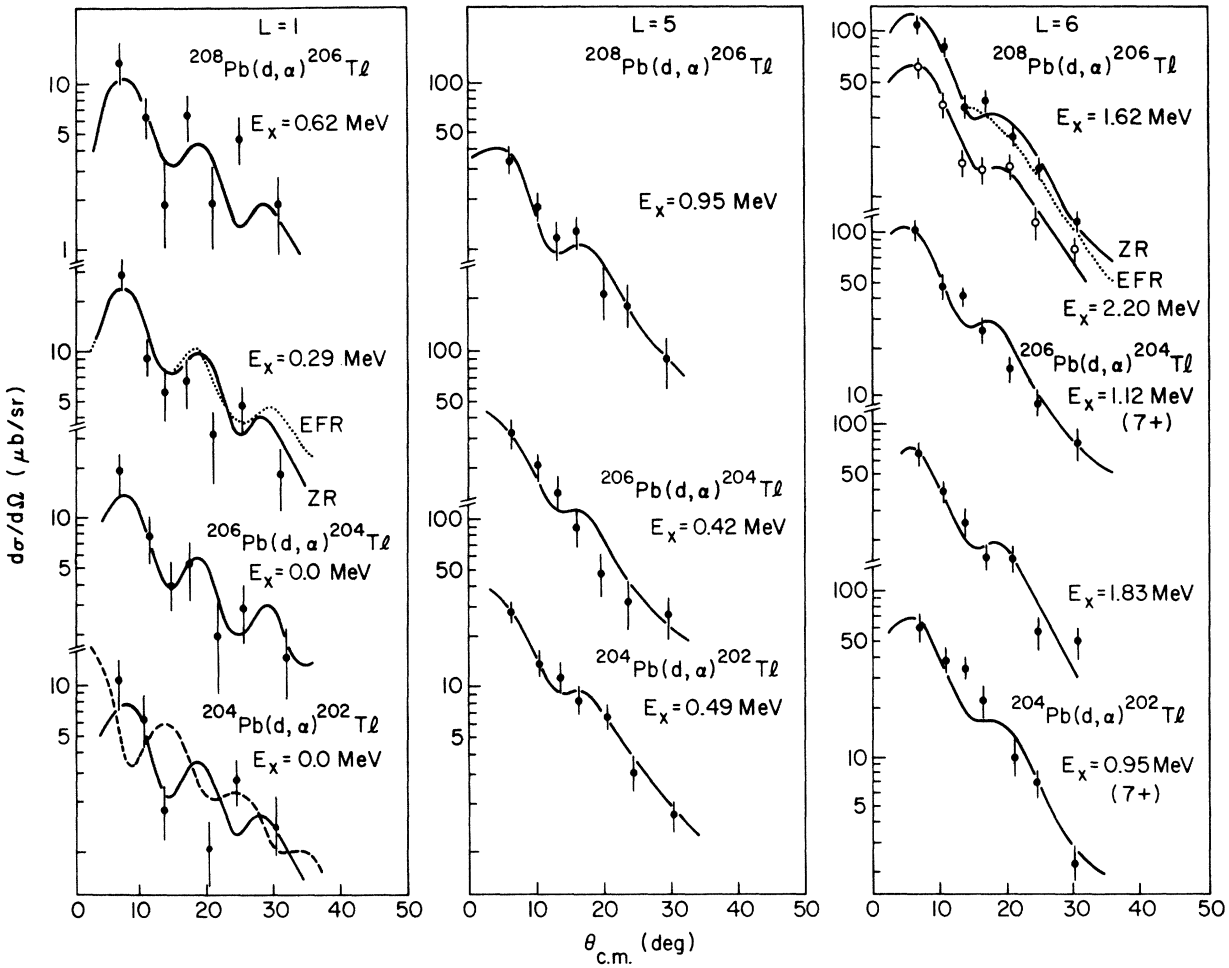


FIG. 2. Comparison of experimental angular distributions and ZR DWBA calculations (solid line) for $L=1$, $L=5$ and $L=6$ transfer. The broken line corresponds to $L=3$ transfer. The dotted lines are EFR calculations.

## IV. ANALYSIS OF $^{208,206,204}$Pb$(d,\alpha)^{206,204,202}$Tl REACTIONS

### A. Distorted-wave Born-approximation calculations

In the following analysis we assume that the $(d, \alpha)$ reaction proceeds through the direct pickup of a neutron and a proton and calculate this process using conventional DWBA techniques.[11,12] As discussed in Refs. 11 and 12 the evaluation of the DWBA amplitude first involves an integration over $\vec{r}_{34}=\vec{r}_3-\vec{r}_4$, the internal coordinate of the deuteron, to yield a range function $D(\vec{r},\vec{s})$ depending upon $\vec{r}=\vec{r}_1-\vec{r}_2$, the separation of the transferred proton and neutron, and $\vec{s}=\frac{1}{2}(\vec{r}_3+\vec{r}_4-\vec{r}_1-\vec{r}_2)$, the separation of the center of mass of the transferred pair from the deuteron center of mass. Specifically, one must evaluate

$$D(\vec{r},\vec{s})=\int \phi_d(\vec{r}_{34})\overline{V}_{10}\phi_\alpha(\vec{r}_{34},\vec{r},\vec{s})d\vec{r}_{34}\,, \qquad (1)$$

where

$$\overline{V}_{10}=V^{10}(r_{13})+V^{10}(r_{14})+V^{10}(r_{23})+V^{10}(r_{24}) \qquad (2)$$

and $V^{10}(r_{jk})$ is an appropriately spin-averaged nucleon-nucleon interaction. It is defined in Appendix A of Ref. 12.

Most of the calculations which follow were carried out using the code DWUCK[13] which employs a zero-range approximation

$$D(\vec{r},\vec{s})\simeq C\exp(-4\eta^2r^2)\delta(\vec{s}) \qquad (3)$$

which is described in detail in the work of Bayman and Kallio.[14] Unfortunately, while this approximation has the merit of calculational simplicity, a simple product of this form is hard to justify theoretically. In addition it is difficult to obtain a realistic estimate for the normalization constant $C$ which is not included in the code.

In view of these problems a limited number of

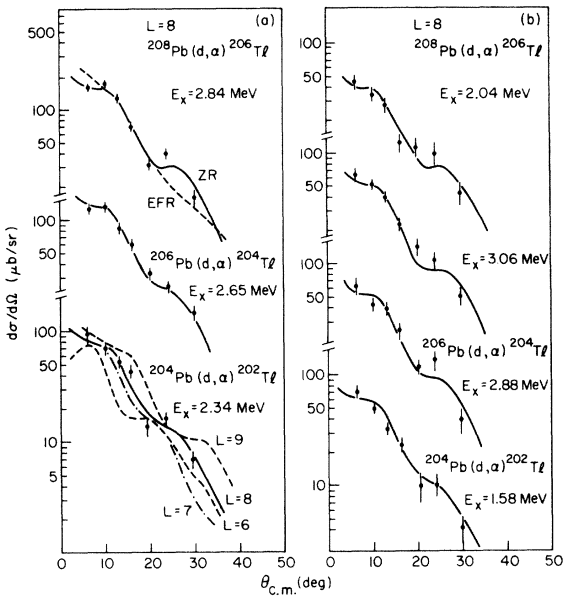


FIG. 3. Comparison of experimental angular distributions and ZR DWBA calculations (solid line) for $L = 8$ transfers. For the transition to the 2.84 MeV level the broken line is an EFR calculation. For the transition to the 2.34 MeV level the broken lines correspond to $L = 6$, 7 and 9 transfers. (a) 9+ levels. (b) Other levels.

exact finite range calculations were carried out in order to investigate the accuracy of the ZR predictions. These calculations were carried out following the multipole expansion technique described by Chant.[12] As was found for the $(t,p)$ and $(p,t)$ transitions studied in Ref. 12 contributions to the DWBA cross sections arising from a multipole expansion of $D(\vec{r},\vec{s})$ converged rapidly. In most cases it was necessary to retain only the monopole term in the expansion. In evaluating $D(\vec{r},\vec{s})$ we used

$$\phi_\alpha(\vec{r}_{34},\vec{r},\vec{s}) = N_\alpha \exp(-2\eta^2 r_{34}^2)\exp(-2\eta^2 r^2)\exp(-4\eta^2 s^2), \quad (4)$$

where $N_\alpha$ is a normalization constant and $\eta = 0.233$ fm$^{-1}$ is consistent with the experimental rms radius for the $\alpha$ particle. The deuteron wave function used was a sum of three Gaussian terms

$$\phi_d(\vec{r}_{34}) = N_d \sum_{i=1}^{3} A_i \exp(-\alpha_i r_{34}^2/4), \quad (5)$$

where $N_d$ is a normalization constant and the other constants, which are given in Ref. 15, lead to a binding energy and rms radius for the deuteron of 2.20 MeV and 1.90 fm in reasonable agreement with the experimental values of 2.22 MeV and 1.95 fm. Finally the nucleon-nucleon interaction used was

$$V^{10}(\vec{r}_{jk}) = -[\tfrac{1}{4}U^{10}(r_{jk}) + \tfrac{3}{4}U^{01}(r_{jk})], \quad (6)$$

where the constants arise from the spin integrations.[12]

The triplet-even interaction was

$$U^{10}(r_{jk}) = 66.92 \exp(-0.415 r_{jk}^2) \text{ MeV} \quad (7)$$

and the singlet-even interaction was

$$U^{01}(r_{jk}) = 29.05 \exp(-0.292 r_{jk}^2) \text{ MeV}, \quad (8)$$

which values[15] are in good agreement with low energy nucleon-nucleon data. No Coulomb term was included for the proton-proton interaction. Since both the $\alpha$ and deuteron wave functions are space symmetric it is unnecessary to specify the interaction in the odd states.

### B. Optical model parameters

Previous $(d,\alpha)$ studies[1,16] have shown that DWBA calculations for this reaction are rather insensitive to the choice of deuteron optical model parameters, whereas a suitable choice among the various optical model parameter families which give good fits to the elastic $\alpha$ channel is crucial for good agreement with experiment.

Deuteron optical parameters were taken from the 80 MeV deuteron elastic scattering survey of Ref. 17. The spin orbit interaction was omitted since it does not affect the $(d,\alpha)$ angular distributions very much.

In order to provide suitable optical parameters for the outgoing channel, the elastic scattering of 92.4 MeV $\alpha$ particles on $^{208}$Pb was measured between laboratory angles of 10° and 55° in 1°

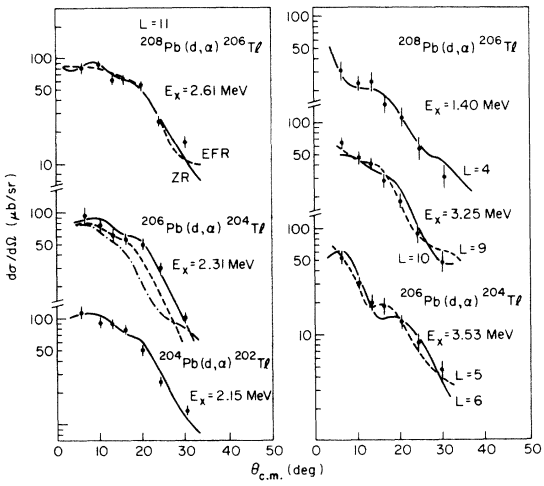


FIG. 4. Comparison of experimental angular distributions and ZR DWBA calculations (solid line). For the transition to the 2.61 MeV level the broken line is an EFR calculation. In addition for the 2.31 MeV level ZR DWBA calculations are shown for $L = 9$ (- • - line) and $L = 10$ (--- line).

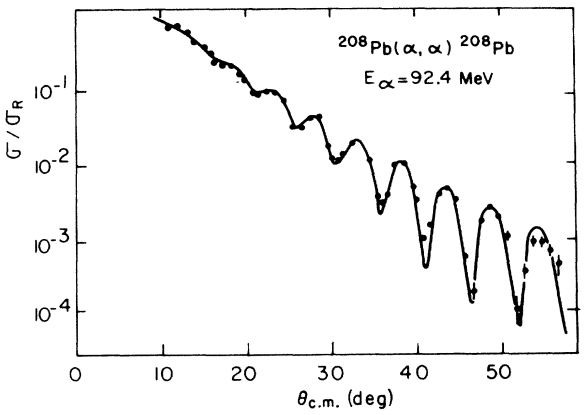


FIG. 5. $^{208}$Pb elastic differential cross section as a ratio to Rutherford scattering. The curve is an optical model fit to the data obtained with the parameter set 5 given in Table I.

steps. The differential cross sections are shown in Fig. 5. Error bars reflect only statistical uncertainties. The absolute error, due mainly to the target thickness uncertainty, is about 20%. An optical model analysis of these data performed with the code JIB3 yielded five different families of optical parameters as indicated in Table I.

Both ZR and EFR calculations utilized single nucleon wave functions generated in Woods-Saxon wells with $r_0 = 1.25$ fm and $a_0 = 0.655$ fm. A spin orbit strength of 25 times the Thomas term was used and the central well depths were adjusted to reproduce one-half of the empirical neutron-proton separation energy. In all cases nonlocality corrections were included with the nonlocality ranges of 0.85 fm for nucleons, 0.54 fm for deuterons, and 0.20 fm for $\alpha$ particles. While the shapes of the predicted angular distributions were not significantly changed by the inclusion of nonlocality corrections the cross sections were found to increase by a factor of 2.

### C. Finite range effects

Initial ZR DWBA calculations using simple single configurations for the transferred nucleons confirmed the sensitivity to the choice of $\alpha$ particle potential previously reported. As shown in Fig. 6 the shallower wells lead to differential cross section predictions quite different from the results obtained using potential sets 4 and 5. Similar behavior has been reported for other transfer reaction DWBA calculations.[18-20] In addition, as mentioned in Ref. 1, a deep $\alpha$ imaginary well seems to be an important ingredient to reproduce experimental angular distributions at 80 MeV.

In common with the analysis of Ref. 1, the calculations shown in Fig. 6 do not take into account finite range effects. Arguably, such effects may be significant at 80 MeV incident energy since, even at forward angles, the relevant transferred momenta (conjugate to the variable $\vec{s}$) are large. In order to investigate this problem EFR calculations were carried out using the computer code TOONA[12] which employs the multipole expansion technique in conjunction with the nucleon-nucleon interaction and light particle wave functions given in Sec. IV A. In the EFR calculations all five potential sets were tried for six values of $L$. Referring to Fig. 6 we recall that in the ZR calculations the various optical parameter sets lead to drastic variations in both shape and magnitude for each $L$ transfer considered. Indeed in some cases, backward peaked curves are obtained in marked contrast to experiment. In Fig. 7, some of the EFR results are shown. These curves are generally qualitatively similar to experiment and vary little in absolute magnitude. Unlike the ZR case the choice of $\alpha$ distorting potential is not especially critical. Best agreement with experiment is in fact obtained using potential set 4 although sets 1 and 5 are almost as good. Presumably the lack of sensitivity of the EFR calculations to the choice of $\alpha$ particle optical potential is a consequence of averaging effects resulting from the finite range function which reduce the importance of the nuclear interior.

### D. Selectivity of the $(d,\alpha)$ reaction at 80 MeV

Both $(d, \alpha)$ and the inverse $(\alpha, d)$ reaction[21-23] are known to populate high spin states preferen-

TABLE I. Optical model parameters used in DWBA calculations.

| Projectile | | $V_R$ (MeV) | $R_R$ (fm) | $A_R$ (fm) | $W_{vol}$ (MeV) | $W_{surf}$ | $R_I$ (fm) | $A_I$ (fm) | $\chi^2/N$ | $J/4A$ | $R_c$ |
|---|---|---|---|---|---|---|---|---|---|---|---|
| $^4$He | 1 | 54.34 | 1.385 | 0.7642 | 24.155 | | 1.492 | 0.6317 | 3.95 | 162.9 | 1.4 |
| $^4$He | 2 | 107.694 | 1.273 | 0.7906 | 20.353 | | 1.504 | 0.6592 | 3.45 | 255.9 | 1.4 |
| $^4$He | 3 | 162.138 | 1.269 | 0.6893 | 22.731 | | 1.415 | 0.8764 | 6.43 | 373.0 | 1.4 |
| $^4$He | 4 | 198.848 | 1.2425 | 0.6959 | 22.871 | | 1.418 | 0.8532 | 6.40 | 431.4 | 1.4 |
| $^4$He | 5 | 245.00 | 1.2345 | 0.668 | 32.649 | | 1.325 | 0.9369 | 7.65 | 477.8 | 1.4 |
| $d$ | 6 | 99.00 | 1.05 | 0.98 | | 25.5 | 1.206 | 0.75 | 25.7 | | 1.4 |

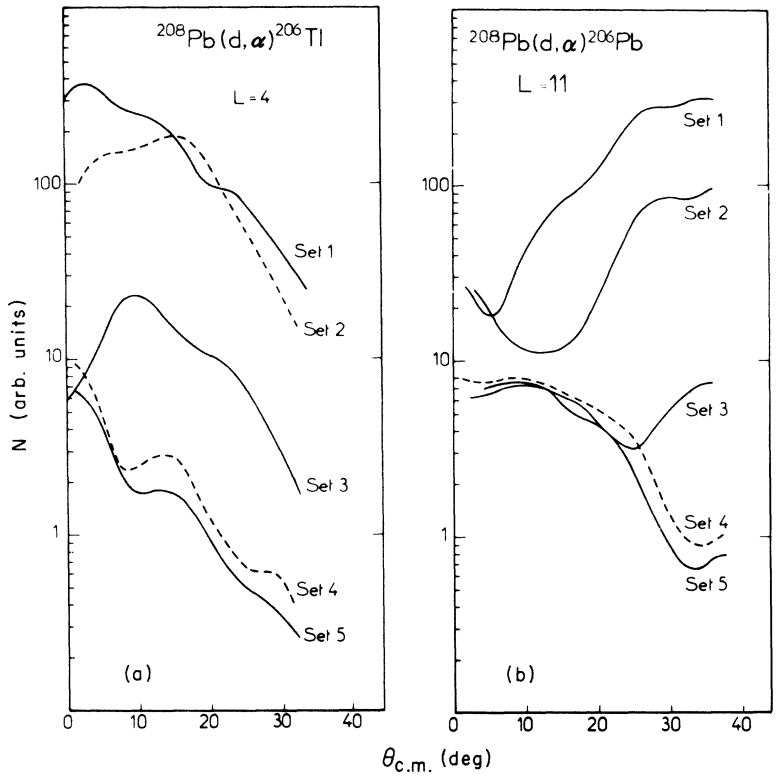


FIG. 6. ZR DWBA calculations using different sets of optical parameters. (a) For an $L=4$ transfer, (b) for an $L=11$ transfer.

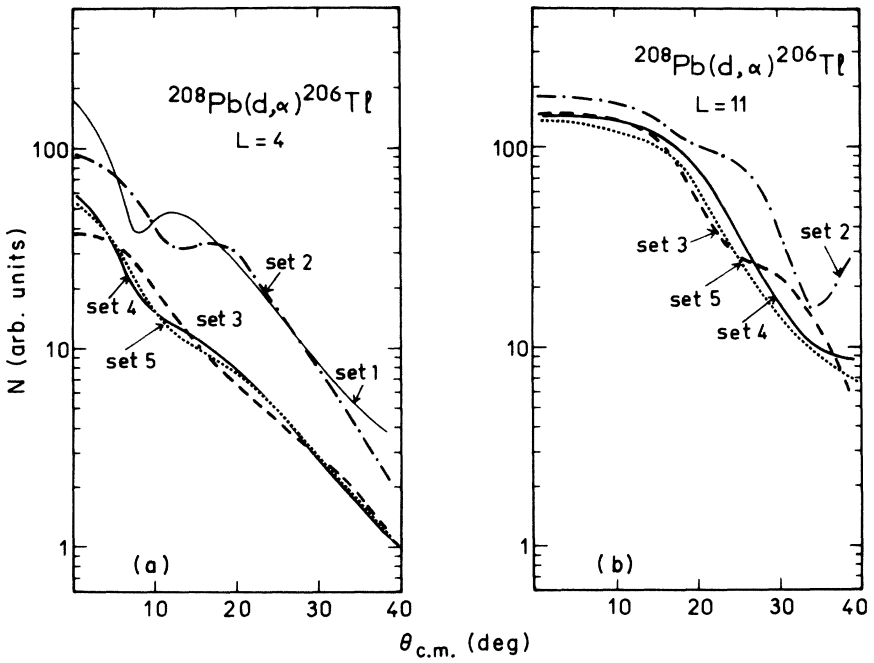


FIG. 7. EFR DWBA calculations using different sets of optical parameters. (a) For an $L=4$ transfer, (b) for an $L=11$ transfer.

tially when the incident energy is chosen to optimize the angular momentum transfer. Thus, at 80 MeV deuteron beam energy angular momentum matching requires that the transferred nucleon pair carries an angular momentum of about $10\hbar$ in the lead region. Large values of $L$ transfer imply large values of the spin $J$ of the residual nuclear states for zero spin targets. Thus, as was shown in Ref. 1, this condition should selectively populate a small number of high $J$ states. Furthermore, the nuclear structure overlap is largest for maximum $J$ in each $\pi^{-1}\nu^{-1}$ configuration. For example, this factor favors $J^\pi = 12^-$ over $J^\pi = 11^-$ by a factor 40 in the case of the $L = 11$ pickup in the $(1i_{13/2}1h_{11/2})$ configuration.

### E. Comparison with angular variation of data

In order to establish $L$-value assignments DWBA calculations were carried out for $^{208,206,204}$Pb$(d, \alpha)^{206,204,202}$Tl assuming various pure configurations $\pi^{-1}(n_1l_1j_1)\nu^{-1}(n_2l_2j_2)$. It was found that, for a given value of $L$, the angular variation of the predicted cross sections was not noticeably altered for different pure configurations. Furthermore, the shapes of the angular distributions were found to characterize the transferred angular momentum $L$ without ambiguity. As one might expect, a strong correspondence appeared between low-lying $^{206}$Tl, $^{204}$Tl, and $^{202}$Tl states since $^{206}$Tl differs from $^{204}$Tl and $^{202}$Tl only by two or four, respectively, additional neutrons. Figure 8 illustrates this phenomenon for corresponding angular distributions of low-lying levels.

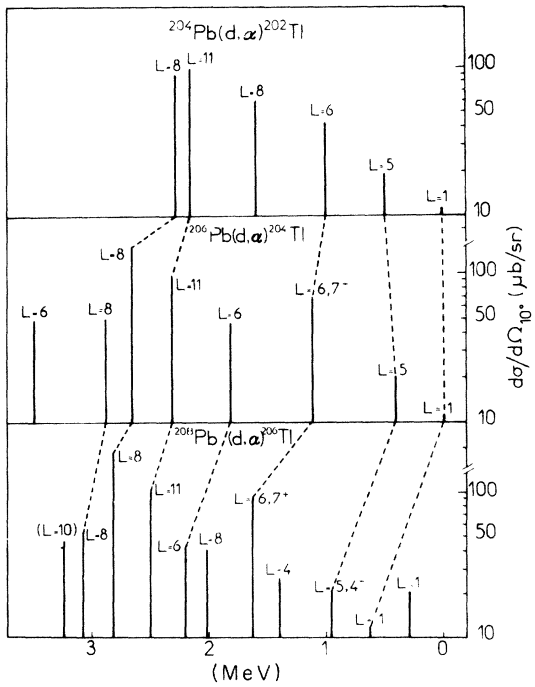


FIG. 8. Identifications of low-lying levels observed in $^{206,204,202}$Tl by $(d, \alpha)$ reactions.

Results are presented in Fig. 2–4 where EFR calculations are shown using $\alpha$ optical potential set 4. As discussed in Sec. IV C the EFR predictions are quite insensitive to this choice and alternative $\alpha$ optical potentials do not change the resultant $L$-value assignments. Since computer time limitations did not permit EFR calculations for all transitions observed ZR results are also included in Figs. 2–4. As is clear from $^{208}$Pb$(d, \alpha)^{206}$Tl results the ZR calculations using potential set 5 reproduce the EFR results quite nicely. Comparable agreement can be expected for the other isotopes. Thus the ZR calculations with an $\alpha$ potential chosen to optimize agreement with the EFR calculations also serve to establish values of the transferred angular momentum $L$.

As expected from the selectivity of the reaction, discussed in Sec. IV D, most of the observed levels have large angular momentum transfer $L$ ($L = 6, L = 8, L = 11$). The principal levels observed were as follows:

#### *1. $L = 11$ transitions—$12^-$ states in $^{206,204,202}$Tl*

States at 2.61 MeV in $^{206}$Tl, 2.31 MeV in $^{204}$Tl, and 2.15 MeV in $^{202}$Tl were found to be strongly populated with similar angular distributions and the same strength. As shown in Fig. 4, only the $L = 11$ calculation correctly reproduces the experimental angular distributions for these levels. According to the selection rules, the corresponding states of the residual nuclei must have either $J^\pi = 10^-$, $11^-$, or $12^-$. The dominant $L = 11$ transition is expected to lead to the $(1i_{13/2}1h_{11/2})^{-1}$ state and the structure factor strongly favors $J^\pi = 12^-$ over $J^\pi = 10^-$ and $11^-$. The ZR DWBA cross sections are 2000 and 300 times lower for $J^\pi = 11^-$ and $J^\pi = 10^-$, respectively, compared with $J^\pi = 12^-$.

Furthermore, as will be shown below, the relative strength and energy for the 2.61 MeV state in $^{206}$Tl compare well with the shell model calculations.[3] Hence, these three states are assigned $J^\pi = 12^-$.

#### *2. $L = 8$ transitions—$9^+$ states in $^{206,204,202}$Tl*

Seven fairly certain $L = 8$ angular distributions in $^{202,204,206}$Tl are seen in Fig. 3. Of these, three, at 2.840 MeV in $^{206}$Tl, 2.65 MeV in $^{204}$Tl, and 2.34 MeV in $^{202}$Tl, are the most strongly populated levels in these reactions. As shown in Fig. 3(a) their shapes are similar and agree well with the DWBA calculations.

While the $L = 11$ transitions have almost identi-

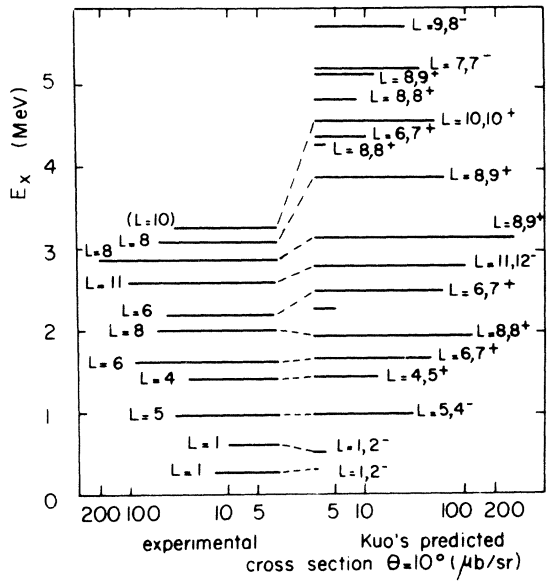


FIG. 9. Comparison of levels and excitation strength predicted in ZR DWBA using Kuo's wave functions with experimental values for the observed levels.

cal cross sections for the three isotopes, the $L = 8$ ones decrease smoothly from $^{206}$Tl to $^{202}$Tl. This behavior is not unexpected since, unlike the $L = 11$ transitions which arise from the single $(1i_{13/2}1h_{11/2})^{-1}$ configuration, many configurations contribute in the $L = 8$ case. Greater changes from isotope to isotope are thus possible. Nevertheless, since the changes in cross section are in fact fairly small, these states are expected to have much the same dominant configurations.

The shell model wave functions of Kuo and Herling predict a very strong $9^+$ excited state at 3.16 MeV with strength and energy in excellent agreement with the $L = 8$ transition at 2.88 MeV in $^{206}$Tl (see Fig. 9). Thus we suggest a $9^+$ assignment for these 3 states.

### 3. *L = 6 transitions*

In Fig. 2 are shown five angular distributions for which $L = 6$ angular momentum transfer has been unambiguously assigned. Three of them, at 1.62 MeV in $^{206}$Tl, 1.12 MeV in $^{204}$Tl, and 0.95 MeV in $^{202}$Tl, are known to be $7^+$ states.[4,9,10] The resulting fit is indeed very good for the first one, but for the two others an $L = 8$ contribution which could explain the discrepancy near 13° is not excluded. In $^{202}$Tl, a close level at 1.098 MeV observed in $\gamma$ ray spectroscopy[9] has been reported with tentative spin assignment $(6^+, 7^+, 8^+)$ compatible with an $L = 8$ DWBA transition and could explain this feature.

### 4. *Other levels*

The well-known low-lying negative parity states $(1^-, 2^-, 4^-)$ have also been observed. As a result of the above discussed $(d, \alpha)$ selectivity, they are weakly excited. However, as shown in Fig. 2, their angular distributions were used as a means of checking the DWBA calculations.

## V. COMPARISON BETWEEN SHELL MODEL CALCULATIONS AND DATA FOR $^{208}$Pb$(d,\alpha)^{206}$Tl

For the $^{208}$Pb$(d, \alpha)^{206}$Tl reaction the data were compared with the results of shell model calculations by Kuo and Herling.[3] In these calculations the Hamada-Johnston potential was used as a residual interaction to generate $\pi^{-1}\nu^{-1}$ wave functions. A first order core polarization correction was also included. Below 4 MeV the predicted levels could be correlated with levels seen in the $(d, \alpha)$ experiment on $^{208}$Pb. These wave functions exhibit extensive configuration mixing, a prediction which seems to be borne out by the present data.

Firstly, ZR DWBA calculations were carried out using the Kuo-Herling wave functions. Since the constant $C$ of Eq. (3) is not included in the code DWUCK a reaction normalization constant $N(d, \alpha)$ needed to convert the output of the code to absolute cross sections was estimated by comparing predicted and measured cross sections for several low-lying states in $^{206}$Tl, particularly the 2.61 MeV $J = 12^-$ level which has a simple $(1i_{13/2}1h_{11/2})^{-1}$ configuration and is the only $12^-$ transition observed. A value of $N(d, \alpha) \sim 800$ was obtained. It should be noted that this result is quite sensitive to the parameters of the calculation. Furthermore, owing to the crude nature of the approximation of Eq. (3) and the difficulty of obtaining a realistic theoretical estimate of $C$, it is our view that no theoretical significance should be attached to the value of $N$ obtained.

In Fig. 9 the ZR DWBA results are compared with our experimental data for $^{208}$Pb$(d, \alpha)^{206}$Tl. The normalization factor obtained above was included and the comparison was restricted to levels with excitation strengths larger than 3 μb/sr at 10° lab. For convenience cross sections are plotted using a logarithmic scale. It is seen that calculation is in fairly good agreement with experiment for levels below 4 MeV excitation. Specifically, several large cross sections resulting from constructive interference of many transition amplitudes are well explained by the shell model wave functions. This is particularly true for the $J^\pi = 9^+$ state at 2.84 MeV. Apart from the strong $J^\pi = 12^-$ state used for normalization, all other negative party states are predicted to be weak, in good agreement with experiment.

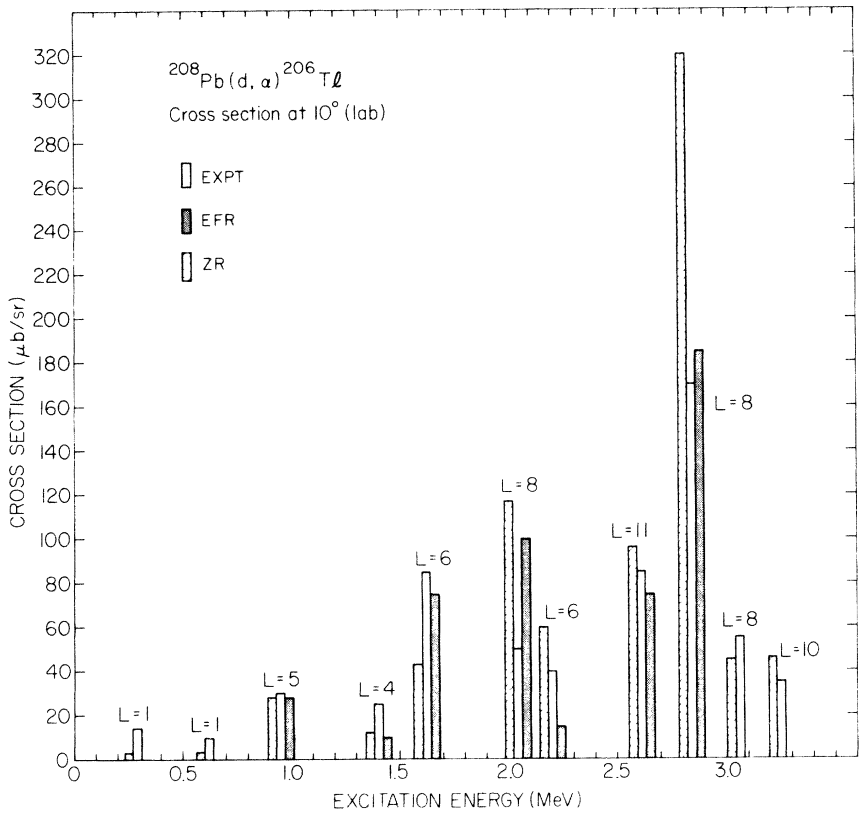


FIG. 10. Comparison of predicted 10° cross sections using Kuo's wave functions with experimental data for $^{208}$Pb-$(d,\alpha)^{206}$Tl. For the ZR DWBA calculations $N(d,\alpha)=800$. For the EFR calculations $N(d,\alpha)=50$.

Above 4 MeV excitation energy, many excited states with small $J$ are predicted to be very weak owing to destructive interference. However, some high spin states are predicted between 4 and 6 MeV excitation with large strength and are not observed experimentally.

Secondly, EFR calculations were carried out using potential set 4 for the seven most strongly excited levels in $^{208}$Pb$(d,\alpha)^{206}$Tl. Using the shell model wave functions of Ref. 3 best agreement with experiment was obtained provided the predicted cross sections were renormalized by a factor $N(d,\alpha)=50$. Predicted EFR cross sections at 10° using this normalization are presented in Fig. 10 together with the corresponding experimental cross sections and ZR predictions taken from Fig. 9. Three results emerge. Firstly, finite range effects are large in the sense that the relative cross sections predicted in EFR are not well described by the ZR results. Secondly, in comparing with experiment, the most notable feature of the EFR analysis is the rather good account given of the relative cross sections for the 4−, 7+, 12− and 9+ levels at 1, 1.68, 2.61, and 2.84 MeV, respectively. Thus, while agreement with experiment is no better in EFR than in ZR for the three other levels studied, we argue that the EFR analysis is somewhat better overall. Thirdly, despite the encouraging results for the relative cross sections it is disappointing to note that the EFR calculations underestimate the observed absolute cross sections by a factor of 50. This may indicate some deficiency in our reaction calculation or perhaps insufficient configuration mixing in the shell model wave functions. It is worth noting that, as is evident from Fig. 7, the problem is not significantly alleviated by using any of the other $\alpha$ optical potential sets listed. Unfortunately large basis shell model studies[24] which do lead to enhancements of as much as an order of magnitude in light nuclei are not as yet available for $^{208}$Pb.

## VI. SUMMARY AND CONCLUSIONS

By taking advantage of the particular selectivity of the $(d,\alpha)$ reaction at 80 MeV in the Pb region we have been able to identify several new high spin states ($J^\pi=12-$ and 9+) between 2 and 4 MeV excitation in $^{202}$Tl, $^{204}$Tl, and $^{206}$Tl. The angular distributions of some of the states observed were com-

pared with EFR DWBA calculations. The results were insensitive to the choice of deuteron and $\alpha$ particle optical potentials. Thus, within the limitations of the DWBA reaction model, $L$-value assignments were unambiguous. Owing to computer time limitations we were obliged to use ZR DWBA calculations for some $L$-value assignments. These calculations reproduced the EFR results closely provided a potential with $V_0 \sim 250$ MeV was chosen from among equivalent $\alpha$ particle optical potentials which reproduced appropriate elastic scattering data but differed by ~50 MeV in real well depth. Thus no additional uncertainty is involved.

For $^{206}$Tl the locations of most of the observed states were found to be in fairly good agreement with the predictions of the Kuo and Herling shell model calculations. In addition the relative $(d, \alpha)$ cross sections are in fair agreement with ZR DWBA calculations using these wave functions. An empirical ZR normalization factor $N(d, \alpha) = 800$ was obtained for the code DWUCK . This is much larger than the value (~20) obtained in Ref. 2 and is particularly sensitive to the choice of $\alpha$ optical potential as well as other details of the calculation such as nonlocality corrections and bound state well parameters.

For seven levels in $^{208}$Pb$(d, \alpha)^{206}$Tl EFR calculations using Kuo's wave functions were carried out. In contrast with the ZR results the choice of $\alpha$ particle optical potential was much less critical and absolute cross sections differed little from one potential choice to another. The EFR calculations lead to improvements in predicted relative cross sections but underestimated absolute cross sections by about a factor of 50. This problem is not understood at the present time and it would be of interest to carry out EFR analyses for other $(d, \alpha)$ transitions.

Finally, we would like to emphasize the unexpected magnitude of the differential cross section for the most strongly populated states. The maximum cross section for the strong levels ($L = 11$ or $L = 8$) is about 100 $\mu$b/sr. Comparable values have been observed for the $L = 6$ transfer in the $(d, \alpha)$ reaction on Ca and Ni and the $L = 9$ transfer on $^{90}$Zr at 80 MeV incident energy. Thus it appears that the effect of angular momentum matching dominates the reaction mechanism in such a way that for well matched transitions the cross section does not decrease with increasing target mass.

ACKNOWLEDGMENTS

We thank very much the University of Maryland cyclotron staff for their comprehensive collaboration. The calculations reported in this paper have been split between three computer facilities: IPN, Orsay (France), Kernforschungsanlage Jülich (Germany), and University of Maryland computer center. We are very grateful to those institutions for generous allocation of computer time. Finally, we are grateful to R. I. Steinberg and J. R. Wu for their able assistance in data taking.

---

*Work supported in part by the U. S. Energy Research and Development Administration.

†On leave from Institut de Physique Nucléaire, 91406 Orsay, France.

[1]N. Frascaria, J. P. Didelez, J. P. Garron, E. Gerlic, and J. C. Roynette, Phys. Rev. C 10, 1422 (1974).

[2]W. C. Parkinson, D. L. Hendrie, H. H. Duhm, J. Mahomey, J. Saudinos, and G. R. Satchler, Phys. Rev. 178, 1976 (1969).

[3]T. T. S. Kuo and G. H. Herling, NRL Memorandum Report No. 2258, 1971 (unpublished).

[4]M. B. Lewis and W. W. Daehnick, Phys. Rev. C 1, 1577 (1970); Phys. Rev. Lett. 22, 77 (1968).

[5]J. R. Erskine, Phys. Rev. 138, B851 (1965).

[6]P. D. Barnes, E. R. Flynn, G. J. Igo, and D. D. Armstrong, Phys. Rev. C 1, 228 (1970).

[7]E. H. Spejewski, Nucl. Phys. A100, 236 (1967).

[8]C. C. Weitkamp, J. A. Harvey, G. G. Slaugter, and E. C. Campbell, Bull. Am. Soc. 12, 922 (1967).

[9]J. Guile, R. E. Doebler, Wm. C. McHarris, and J. H. Kelly, Phys. Rev. C 5, 2107 (1972).

[10]R. L. Auble and M. J. Martin, Nucl. Data B5, 582, 602 (1971).

[11]I. S. Towner and J. C. Hardy, Adv. Phys. 18, 401 (1969).

[12]N. S. Chant, Nucl. Phys. A211, 269 (1973).

[13]DWUCK4 is an unpublished computer program kindly made available to us by P. D. Kunz of the University of Colorado.

[14]B. F. Bayman and A. Kallio, Phys. Rev. 156, 1121 (1967).

[15]F. S. Chwieroth *et al.*, Nucl. Phys. A189, 1 (1972).

[16]R. M. Del Vecchio and W. W. Daehnick, Phys. Rev. C 6, 2095 (1972).

[17]G. Duhamel, L. Marcus, H. Langevin-Joliot, J. P. Didelez, P. Narboni, and C. Stephan, Nucl. Phys. A174, 485 (1971).

[18]J. P. Didelez *et al.*, Phys. Rev. C 13, 1388 (1976).

[19]J. R. Shepard, P. D. Kunz, and J. J. Kraushaar, Phys. Lett. 56B, 135 (1975).

[20]E. Gerlic, J. Van de Wiele, H. Langevin-Joliot, J. P. Didelez, G. Duhamel, and E. Rost, Phys. Lett. 52B, 39 (1974).

[21]M. J. Spisak, W. W. Daehnick, W. Oelert, and R. M. Del Vecchio, Bull. Am. Phys. Soc. 20, 670 (1975).

[22]C. C. Lu, M. S. Zisman, and B. G. Harvey, Phys. Rev. 186, 1086 (1969).

[23]R. M. Del Vecchio, R. T. Kouzes, and R. Sherr, Nucl. Phys. A265, 220 (1976).

[24]See for example D. H. Feng, R. H. Ibarra, and M. Vallieres, Phys. Lett. 46B, 37 (1973). D. H. Feng *et al.*, Phys. Rev. C 14, 1484 (1976).

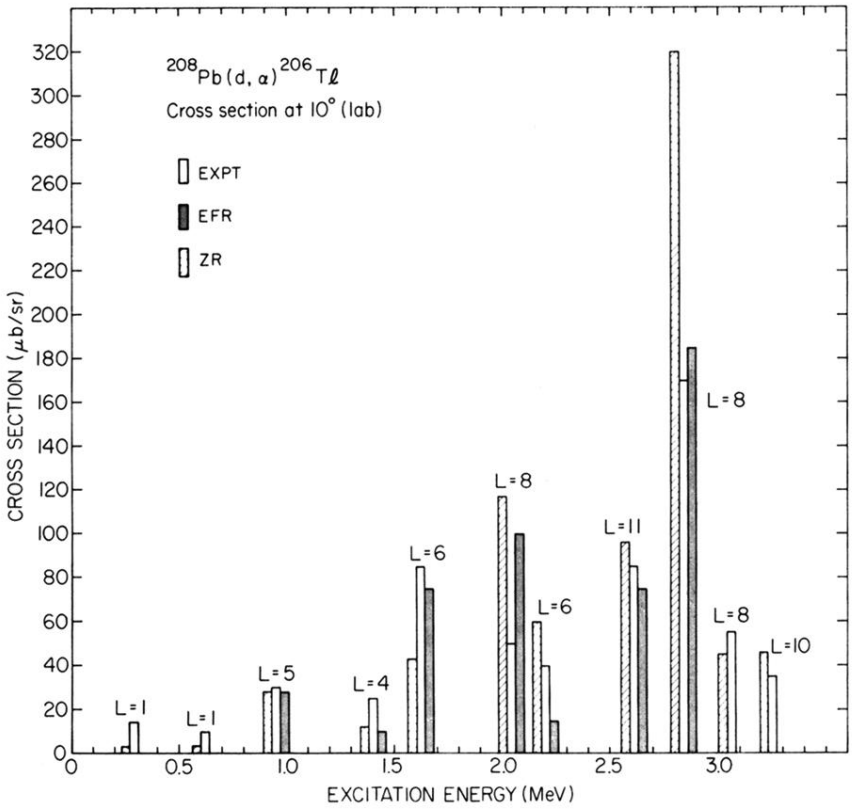


FIG. 10. Comparison of predicted 10° cross sections using Kuo's wave functions with experimental data for $^{208}$Pb-$(d,\alpha)^{206}$Tl. For the ZR DWBA calculations $N(d,\alpha)=800$. For the EFR calculations $N(d,\alpha)=50$.